Probing Secondary Coordination Sphere interactions within Porphyrin-Cored Polymer Nanoparticles

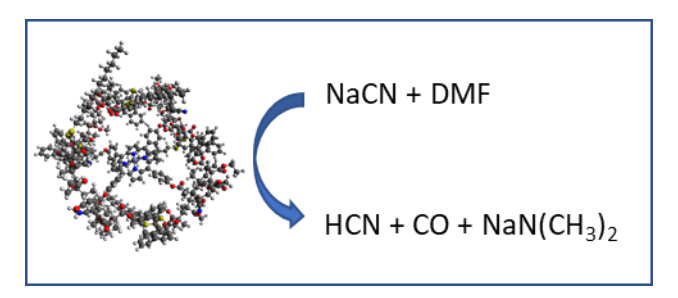
Brian F. Patenaude[†], Erik B. Berda^{†‡}, Samuel Pazicni^{*}

* Department of Chemistry, University of Wisconsin–Madison, 1101 University Avenue, Madison, Wisconsin 53706, United States

†Department of Chemistry and ‡Materials Science Program, University of New Hampshire, 23 Academic Way, Durham, New Hampshire 03824, United States

TABLE OF CONTENTS GRAPHIC (For Table of Contents use only)

TOC (Color)-3.25 wide x 1.375 in. high



"Secondary coordination sphere interactions of zinc porphyrin-cored polymers and nanoparticles were explored via their catalysis of the reaction between cyanide and N,N-dimethylformamide. Nanoparticle structure modeled by optimizing geometries with universal force fields (UFF) in Avogadro."

A suite of zinc porphyrin-cored random coil polymers and polymeric nanoparticles with varying degrees of potential hydrogen bonding character and steric bulk were synthesized and characterized to study secondary coordination sphere interactions. The reaction of cyanide with N,N-dimethylformamide in the presence of porphyrin-cored polymeric nanoparticles was monitored via UV-Vis spectroscopy. It is shown that the zinc porphyrin-cored polymers and nanoparticles catalyzed the reaction of cyanide with N,N-dimethylformamide with the highest reaction rates occurring with polymeric nanoparticles with a greater number of potential hydrogen bond donors and greater steric bulk.

KEYWORDS biomimetic; reversible addition fragmentation chain transfer; metal-polymer complexes; organometallic catalysts; porphyrin-enzyme models; UV-VIS spectroscopy; Diffusion ordered spectroscopy

1. Introduction:

In nature, porphyrin cofactors within heme proteins allow for a wide variety of functions including oxygen transfer (myoglobin, hemoglobin), electron transfer (cytochrome c, cytochrome b_5), catalysis (peroxidase and cytochrome P450), and signaling (CooA).^{1–3} While the function of heme proteins are often

governed by the axial ligands of the iron porphyrin cofactor,² non-covalent secondary coordination sphere interactions play a significant role in the activity of these proteins.⁴ For example, the secondary coordination sphere interactions of the distal amino acid residue of myoglobin and hemoglobin which enhance the

reversible binding of O_2 while lowering CO affinity.^{5–7}

The stabilization of dioxygen coordination in hemoglobin through a secondary coordination sphere interaction via hydrogen bonding of a distal histidine was first suggested by Pauling in 1964.8 Early attempts to synthesize dioxygen bound iron porphyrin were met with some success. 9-14 But, the isolation of a dioxygen bound model complex was not reported until 1975 with the synthesis of meso-tetra($\alpha,\alpha,\alpha',\alpha$ o-pivalamidophenyl)porphyrin, "picket fence" porphyrin, by Collman and coworkers. 15 The steric bulk of the pivalamide groups of the picket fence porphyrins generate an aprotic cavity allowing for the preferential binding of a bulky imidazole to the unhindered side of the porphyrin while reversibly binding O2 in the cavity. X-ray crystallography of the picket fence porphyrin showed the N-H groups of pivalamide facing inward toward dioxygen but the distance to the terminal oxygen was too great to allow for hydrogen bonding.¹⁵ Further work by Collman and coworkers in 1994, sought to elucidate the role of H-bond and dipole-dipole interactions in the heme enzymes through the binding of O₂ to "Picnic Basket" porphyrins of varying cavity size. Collman and coworkers were able to indicate a dipole-dipole interaction between the amide protons and the bound O₂ by an increase in O₂ affinity as "picnic basket" cavity size decreased. 16 While the "picket fence" and "picnic basket" porphyrins allowed for the study of secondary coordination sphere interactions, the proximity of the amide protons did not allow for H-bonding nor did their designs fully replicate the enveloping macromolecular environment found in the native proteins.

While heme-peptide models have been produced as a means to study heme models in a macromolecular environment, their synthesis are complex and challenging. ^{17,18} An alternative method to incorporate porphyrin into a

macromolecular environment is the inclusion of porphyrin into a polymer scaffold. Porphyrin has previously been incorporated into several polymeric systems.¹⁹ Recently polymeric porphyrin systems have shown viability as peroxidase enzyme mimics²⁰ and potential antitumor agents²¹. Of particular relevance to this study is a series of tetra-functionalized iron porphyrin cored star polymers (PCSPs) designed and synthesized by Rodriguez and coworkers, amenable to post polymerization modification to form nanoparticles (PCNPs). The PCSPs and PCPNs exhibited similar redox and ligand binding behavior to that of native heme proteins.^{22,23} While the polymer scaffold of the PCPNs synthesized by Rodriguez and coworkers were shown to protect the iron-porphyrin core from dimerization there was little evidence of secondary coordination sphere interactions. 22,23

$$X = \begin{cases} O \\ N \\ N \end{cases} = \begin{cases} N \\ N \\ N \end{cases} = N \end{cases} = \begin{cases} N \\ N \\ N \end{cases} = N \end{cases} = \begin{cases} N \\ N \\ N \end{cases} = N \end{cases} = \begin{cases} N \\ N \\ N \end{cases} = N \end{cases} = N \\ N \\ N \end{cases} = N \end{cases} = N \\ N \\ N \\ N \end{cases} = N \end{cases} = N \\ N \\ N \\ N \end{cases} = N \end{cases} = N \\ N \\ N \\ N \end{cases} = N \end{cases} = N \\ N \\ N \\ N \end{cases} = N \\ N \\ N \\ N \end{cases} = N \\ N \\ N \end{cases} = N \\ N \\ N \\ N \end{cases} = N \\ N \\ N \end{cases} = N \\ N \\ N \\ N \end{cases} = N \\ N \\ N \\ N \end{cases} = N \\ N \\ N \\ N \end{cases} = N \\ N \\ N \\ N \end{cases} =$$

Figure 1: Suite of zinc porphyrin cored star polymers of varying degrees of possible hydrogen bonding character and steric

properties for probing secondary sphere interactions.

In the present study a series of porphyrin cored star polymers and polymeric nanoparticles of varying degrees of potential hydrogen bonding character and steric properties including $Zn^{\parallel}(por[poly(MMA-co-AMMA)]_4)$ {PCSP-1 : PCPN-1}, Zn^{II}(por[poly(HexMAAm-co-{PCSP-2 Zn^{II}(por[poly(iPMAAm-co-AMMA)]₄) {PCSP-3 : PCPN-3}, and Zn^{II}(por[poly(HEMA-co-AMMA)]₄) {PCSP-4 : PCPN-4} were synthesized as abstractions of heme proteins (Figure 1). These polymeric systems were designed to further explore the viability of PCSPs and PCPNs as model complexes of heme proteins. In the present study, cyanide was utilized as a molecular probe to explore the secondary coordination sphere interactions of the polymer scaffold with the porphyrin core (Figure 2). In preliminary UV-vis spectroscopy studies, the various Zn-Porphyrin-cyanide systems were found to have varying reactivities with the solvent dimethylformamide (DMF).

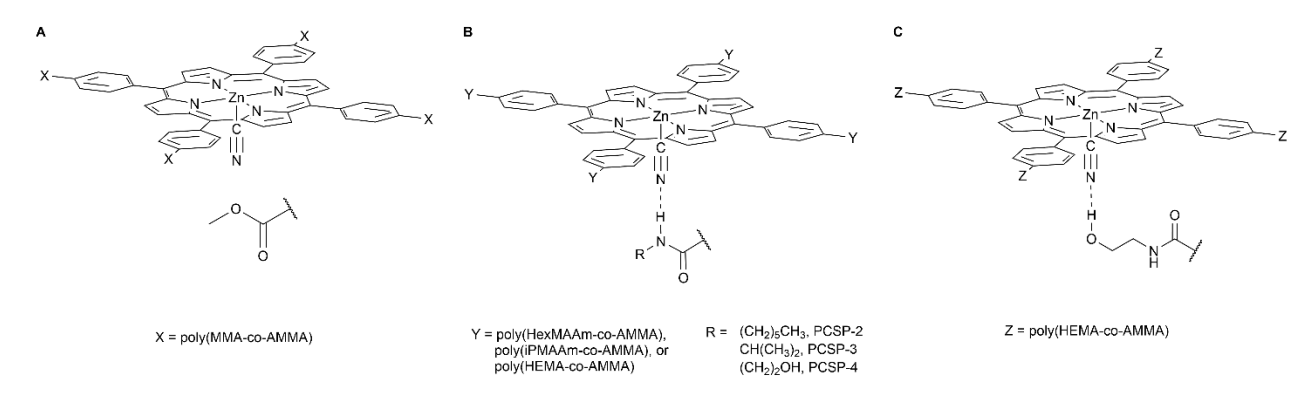


Figure 2: Possible secondary coordination sphere interactions of the porphyrin cored polymers. (A) The ester functional groups of the poly(MMA-co-AMMA) scaffold were expected to have limited interactions with the bound cyanide. (B) The amide functional groups of the polyacrylamide polymer scaffolds would

allow for the possibility of N-H···N hydrogen bonds with the bound cyanide. (C) The hydroxyl groups of the poly(HEMA-co-AMMA) scaffold would allow for the possibility of O-H···N hydrogen bonds with the bound cyanide.

2. Results and Discussion

2.1 Polymer Design and Synthesis

To generate the polymeric scaffolds for probing secondary sphere interactions, por[poly(MMA-co-AMMA)]₄ por[poly(PFPMA-co-AMMA)]₄ were synthesized by reversible addition-fragmentation chain transfer (RAFT) with 5,10,15,20-tetrakis(4-(4cyano-4-[(dodecylsulfanylthiocarbonyl)sulfanyl]phenyl pentanoate)-21H,23H-porphine (PorCTA) the chain transfer agent azobisisobutyronitrile (AIBN) as the radical initiator. The method of RAFT polymerization using a thiocarbonylthio chain transfer agent was chosen for this study as this method of polymerization allows for predictable molecular weights and narrow polydispersities.^{24,25} In por[poly(MMA-co-AMMA)]₄, methacrylate was chosen as a monomer in order to synthesize a polymer scaffold which was not expected to strongly interact with the zincbound cyanide (Figure 2A). 9-Anthracenylmethyl methacrylate was incorporated into the polymer scaffold of all polymer species in this study to allow for nanoparticle formation through the photo induced dimerization of the anthracene units.²⁶ Pentafluorophenyl methacrylate was incorporated as it has previously been shown to allow for post-polymerization modification through nucleophilic acyl substitution with amines leading to polymer scaffolds with possible hydrogen bond acceptors and donors.^{23,27} Por[poly(MMA-co-AMMA)]₄ and por[poly(PFPMA-co-AMMA)]₄ characterized by absorption spectroscopy and ¹H NMR. Por(MMA-co-AMMA)₄ was obtained at M_n = 17.2 kDa with a 22.8% AMMA incorporation and 26.5 monomer units per arm on average based on ¹H NMR (ESI-Figure S9). The molecular weight of por[poly(MMA-co-AMMA)]₄ was chosen to match the molecular weight of horse myoglobin, 16.95 kDa.²⁸ Por[poly(PFPMA-co-AMMA)]₄ was obtained at 33.2 kDa with a 14.6% AMMA incorporation and 30.2 monomer units per arm on average based on ¹H NMR (ESI-Figure S11). Por[poly(PFPMA-co-AMMA)]₄ was formulated such that the AMMA incorporation and number of monomer units in each arm would be similar to those of the aforementioned por[poly(MMA-co-AMMA)]₄ species.

Zinc was chosen as the coordinating metal for this study as zinc porphin is known to be diamagnetic allowing for NMR studies. As cyanide is highly toxic and lethal, zinc porphin complexes have previously been designed as cyanide sensors and shown to bind cyanide. ^{29,30} Insertion of Zn^{II} into por[poly(MMA-co-AMMA)]₄ and por[poly(PFPMA-co-AMMA)]₄ via the reaction with zinc acetate was confirmed by the contact shift of the pyrrole ¹H-NMR signal (from 8.87 to 8.93 ppm, ESI-Figures S14 & S18) and the anticipated change in the Soret (418 to 426 nm), and α,β absorbance signatures (514, 549, 592, and 649 nm to 559 and 599 nm, ESI-Figures S15 & S19).

In order to generate the possibility of N-H...N hydrogen bonds forming between the polymer scaffolds and the cyanide adduct (figure 2B), PCSP-2, PCSP-3, and PCSP-4 were the synthesized by post-polymerization Zn"(por[poly(PFPMA-comodification of AMMA)]₄) through nucleophilic acyl substitution carried out in dimethyl sulfoxide (DMSO) using hexan-1-amine, propan-2-amine, aminoethanol, respectively. Hexan-1-amine was chosen due to its large nonpolar chain and its moderate steric properties. Similarly, Propan-2amine was chosen to produce a species which generates hydrophobic environments while having greater stearic bulk compared to hexan1-amine due to the branched nature of propan-2-amine. 2-Aminoethanol was chosen for nucleophilic acyl substitution to incorporate serine-like motif which may generate the possibility of O-H···N hydrogen bonds between the polymer scaffold and the cyanide adduct (Figure 2c). Completion of nucleophilic acyl substitution was confirmed by the loss of pentafluorophenol via ¹⁹F NMR (ESI-Figures S21, S25, & S29) and the growth of the associated amide proton ¹H-NMR signals (ESI-Figures S20, S24, S28).

2.2 Nanoparticle Fabrication and Characterization by DOSY NMR

PCPNs were synthesized from the parent polymers by the dimerization of the anthracene units under dilute conditions in DMF through photoinduced $[4\pi + 4\pi]$ cycloaddition ($\lambda = 350$ nm).²⁶ Collapse of the polymer species were monitored by the decrease in the anthracene absorption signature as well as through ¹H-NMR, gCOSY, and DOSY NMR. Two hours of UV exposure (λ = 350 nm) lead to a 52 ± 2 % conversion of anthracene to the anthracene dimer in PCPN-1, $47 \pm 3 \%$ in PCPN-2, 40.8 ± 0.02 % in PCPN-3, and 70 ± 4 % in PCPN-4, calculated from the change in absorbance at 366.5 nm. Formation of the anthracene dimer indicating nanoparticle formation was confirmed by the change in coupled aromatic ¹H NMR chemical shifts ({8.34, 7.70}, {8.29, 8.00}, {8.19, 7.60} and {7.63, 7.40} to {8.38, 8.28}, {8.30, 8.00}, {8.23, 8.17} and {8.15, 8.06}, gCOSY NMR, 400 MHz, DMF-d₇, ESI-Figure S39).

Exposure of the polymer species to UV radiation over 2 hours generated several nanoparticle species of varying size. The Stokes or hydrodynamic radius, R_H , of the parent polymers and nanoparticles were calculated using the Stokes-Einstein equation (Equation 1). Where k_b is the Boltzmann constant, T is the absolute temperature, D is the diffusion constant, and η is the solutions viscosity.

$$R_H = \frac{k_B T}{6\pi \eta D} \tag{1}$$

The diffusion constants, D, were obtained through Bayesian transformation using Mestrelab Mnova NMR Software (Ver. 14.0.0) of DOSY NMR data obtained from diffusion experiments in DMF-D7 at 298 K. Based on DMF's viscosity of 0.802 cP at 25 °C, 33 R_H of PCSP-1 decreased from 31.3 to 15.5 Å during the formation of PCPN-1 (ESI-Figures S16 & S43). RH of PCSP-2 decreased from 20.5 to 17.0 Å during the formation of PCPN-2 (ESI-Figures S23 & S44). R_H of PCSP-3 changed from 27.5 to 27.7 Å during the formation of PCPN-3 (ESI-Figures S27 & S45). R_H of PCSP-4 decreased from 31.8 to 21.1 Å during the formation of PCPN-4 (ESI-Figures S31 & S46). There was no apparent sign of intermolecular crosslinking during nanoparticle formation as there were no species detected via DOSY NMR with greatly increased hydrodynamic radius compared to the parent polymer. The differences in hydrodynamic radius of the collapsed nanoparticles may be indicative of the differences in steric hindrance inherent in each of the species, but this will require additional molecular dynamic simulations to say with certainty.

2.3 Zinc-Porphyrin Cyanide Binding Studies

The binding of cyanide was confirmed and monitored via UV-vis spectroscopy. Binding of cyanide was completed by spiking a stock solution of sodium cyanide in DMF (4.4 mg/mL) into aliquots of polymer in DMF solution with a final concentration of ~3 μ M Polymer and 0.5 mM NaCN. Binding of cyanide was confirmed and monitored by anticipated changes in the Soret, α , and β absorbances signatures. Upon addition of sodium cyanide solution to the polymer solutions the Soret peak immediately shifted from 429 to 439 nm. The α , β peaks shifted from 562 and 604 to 581 and 625 nm matching previously reported systems and indicating the formation of a Zn-porphyrin

cyanide adduct (ESI-Figures S47 to S54).^{29,30} Observing the UV-vis spectrum of PCSP-1,PCPN-1, and PCSP-2 peak over several hours (figures S54 to S56) it was found that the zinc-cyanide adduct was unstable over time with decreases in absorbance at 439, 581 and 625 nm and increases in absorbance at 428.5, 562 and 604 nm with isosbestic points occurring at 433.5, 569.5, 595.5 and 611.5 nm (ESI-Figure S55).

Past experiments by Ram Chand Paul and B. R. Sreenathan have previously shown that metal cyanides slowly react with DMF to form metal dimethylamines, carbon dioxide, and hydrogen cyanide under reflux conditions (Equation 2).³⁴

NaCN + H
$$\stackrel{O}{\longmapsto}$$
 HCN + CO + NaN(CH₃)₂ (2)

Testing for the presence of HCN via the titration of PCPN-4 test solution two weeks after sodium cyanide addition with sodium acetate led to the partial recovery of the characteristic 439, 581 and 625 nm absorption peaks associated with

the cyanide adduct (ESI-Figure S58). As the absorbance peak at 625 nm was recoverable, it was hypothesized that the zinc porphyrin substrates were acting as catalysts for the reaction of cyanide and DMF at room temperature.

To elucidate reaction kinetics, the UV-Vis absorbances at 428.5 and 439 nm were monitored for 24 hours after sodium cyanide addition to a degassed solution of polymer at 25 °C with absorbance measurements taken every 15 minutes. Replicating the experiments in triplicate for each polymer species resulted in the intensity of absorbance at 439 nm diminished at varying rates depending on polymer scaffold functionality and topology (Figure 3). Twenty-four hours after sodium cyanide addition the absorbance at 439 nm decreased by 4.0 ± 0.1 % for PCSP-1, 9 ± 2 % PCPN-1, 18 ± 7 % for PCSP-2, 30 ± 10 % for PCPN-2, 36 ± 7 % for PCSP-3, 50 ± 10 % for PCPN-3, 33 \pm 9 % for PCSP-4, and 43 \pm 2 % for PCPN-4 (Table 1).

	Random Coil (PCSP)			Folded Particle (PCPN)		
Polymer Species	\overline{D} (cm ² /s)	<i>R̄_H</i> (Å)	-Δ Abs @ 439 nm [24 h]	\overline{D} (cm ² /s)	R̄ _H (Å)	-Δ Abs @ 439 nm [24 h]
Zn"(Por[poly(MMA-co-AMMA)] ₄)	8.70e-7	31.3	3.9 ± 0.2 %	1.76e-6	15.5	9 ± 2 %
Zn ^{II} (Por[poly(HexMAAm-co- AMMA)] ₄)	1.33e-6	20.5	18 ± 7 %	1.60e-6	17.0	30 ± 10 %
Zn ^{II} (Por[poly(iPMAAm-co- AMMA)] ₄)	9.92e-7	27.5	36 ± 7 %	9.82e-7	27.7	50 ± 10 %
Zn"(Por[poly(HEMA-co- AMMA)] ₄)	8.57e-7	31.8	33 ± 9 %	1.29e-6	21.1	43 ± 2 %

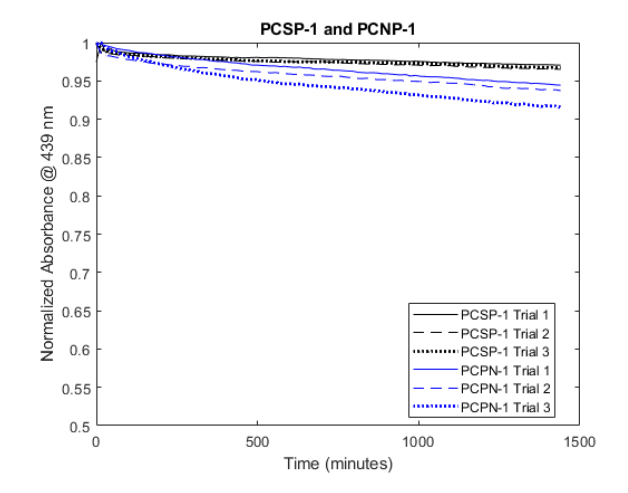
Table 1: Diffusion constants, Stokes radius, and average percent change in Soret UV-Vis absorbance at 439 nm associated with the Zn-porphyrin-CN adduct 24 hours after cyanide addition for the random coil and folded particle polymer specie.

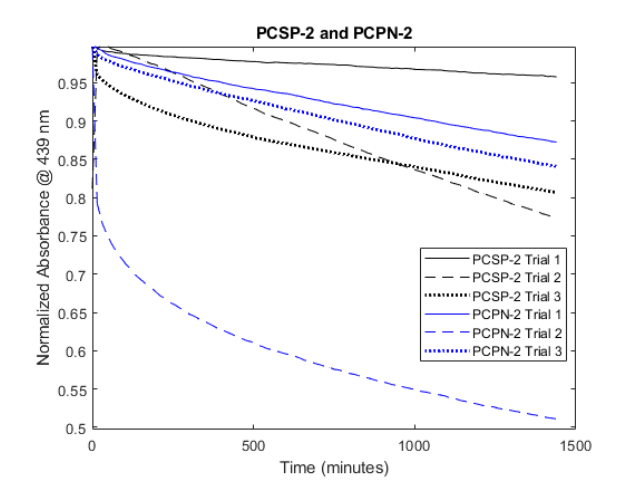
In the comparison of each random coil (PCSP) species with their associated folded particles (PCPN), the nanoparticles presented a quicker

decrease in measured absorbance than their random coil parent species (Table 1). This indicates that the proximity of the polymer arms

from the porphyrin core may be pivotal to the observed reaction. Comparison hydrodynamic radius of the random coil configurations of PCSP-1, 31.3 Å, and PCSP-4, 31.8 Å, may insinuate that PCSP-1 and PCSP-4 are solvated to a similar degree. Yet, upon addition cyanide, PCSP-4 decreases characteristic 439 nm absorption peak associated with the cyanide adduct at a greater rate than PCSP-1 with changes in absorbances of $33 \pm 9 \%$ and $3.9 \pm 0.2 \%$ on average in a 24-hour period. This may be indicative that the presence of possible hydrogen bonds increases reaction rates. In addition, within the acrylamide folded particle species a trend is observed in which rate of change increases with increases in hydrodynamic radius. With the absorbance at 439 nm of PCPN-2, PCPN-4, and PCPN-3 decreasing by $30 \pm 10 \%$, $43 \pm 2 \%$, and $50 \pm 10 \%$

respectively over a 24-hour period. However, due to the large error in the measurements the differences between the changes in absorbances of PCSP-3 and PCSP-4 as well as between PCNP-3 and PCNP-4 cannot be fully differentiated. This trend was not observed in the random coil In each configuration ZnII(Por[poly(iPMAAm-co-AMMA)]4) species which was expected to have the greatest steric properties resulted in the greatest rate of reaction. These relative changes in absorbance at 439 nm, indicates that polymers with a greater number of potential hydrogen bond donors and greater steric bulk increased the rate of the observed reaction. The absorbance data at 439 nm for these reactions (Figure 3) could not be linearly fit for 1st or 2nd order kinetic models, presenting the possibility of concurrent reactions.





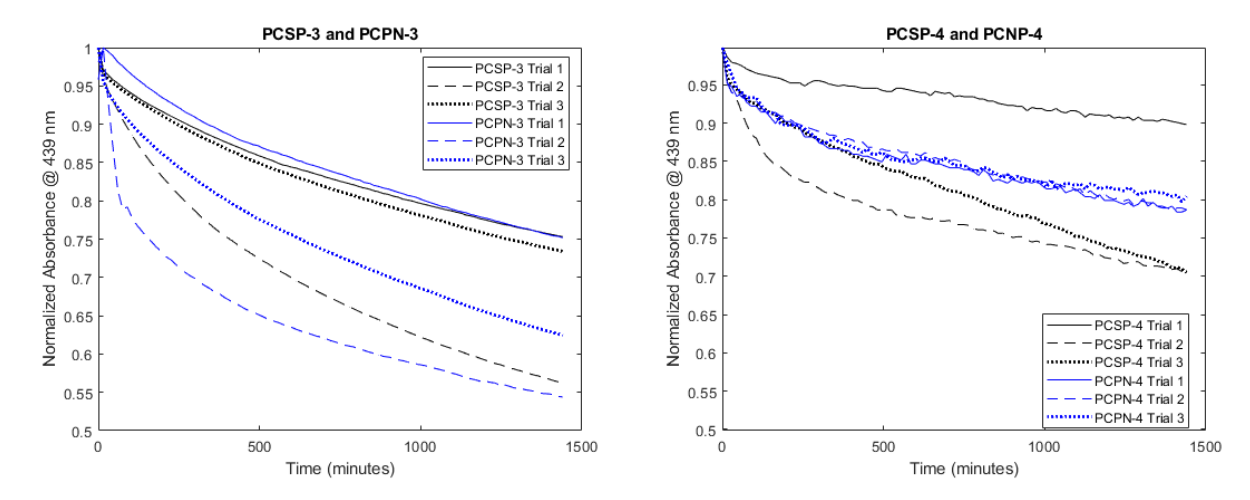


Figure 3: Normalized absorbance over 24 hours after cyanide addition to PCSP-1 (Black), PCPN-1 (Blue), PCSP-2 (Black), PCPN-2 (Blue), PCSP-3 (Black), PCPN-3 (Blue), PCSP-4 (Black), PCPN-4 (Blue). Absorbance data normalized to greatest absorbance measured during each trial.

2.4 Isolation and Characterization of the Byproduct of the Zinc-Porphyrin Cyanide Reaction.

To isolate the products of the reaction sodium between cyanide and N,Ndimethylformamide in the presence of the zinc porphyrin polymers, a large excess of sodium cyanide was added to a dilute solution of PCPN-2 in DMF and stirred under ambient conditions. 48 hours after the sodium cyanide addition a white precipitate was isolated and characterized by ¹H NMR, ¹³C NMR and ATR-IR. A lack of a ¹H NMR signal (ESI-Figure S60) in conjunction with a single 168.08 ppm ¹³C NMR chemical shift in D₂O (ESI-Figure S61) indicated that sodium dimethylamine was not present. Comparison of the IR spectra of the precipitate (ESI-Figure S62) with commercially available sodium carbonate (ESI-Figure S63) lead to the identification of the solids as sodium carbonate.

The reaction of hydroxide ions with carbon dioxide leading to the subsequent generation of carbonate in aqueous media (equations 5 and 6) has been previously studied

by Pohorecki and Moniuk.³⁵ Due to the possible absorption of atmospheric moisture and carbon dioxide into DMF under ambient conditions it is proposed that the following cascade of reactions occurred following the reaction of cyanide and DMF resulting in the accelerated formation of sodium carbonate.

$$NaN(CH_3)_2 + H_2O \implies HN(CH_3)_2 + NaOH$$
 (3)

NaOH + H
$$\stackrel{O}{\longrightarrow}$$
 H₂O + CO + NaN(CH₃)₂ (4)

$$NaOH + CO_2 \longrightarrow NaHCO_3$$
 (5)

$$NaHCO_3 + NaOH \implies Na_2CO_3 + H_2O$$
 (6)

Scheme 1: Subsequent reactions occurring during the reaction of sodium cyanide and DMF in the presence of zinc porphyrins under ambient conditions.

To test the hypothesis that the polymer species were catalyzing the reaction of cyanide with DMF, the folded particles of each polymer species and a control of DMF were reacted with

large excesses of cyanide over 48 hours under ambient conditions in triplicate. The resulting percent yields of sodium carbonate were 78.7 ± 0.7 , 81 ± 6 , 83 ± 2 , and 74 ± 1 % for PCPN-1, PCPN-2, PCPN-3, and PCPN-4 respectively. There was a yield of 68 ± 2 % of sodium carbonate for the control containing only DMF and cyanide. Replication of the experiments replacing cyanide with acetate lead to the recovery of starting material only. This indicates that the cyanide does react with DMF at room temperature and the polymers are increasing the rate of dimethylamine generation resulting in larger yields of sodium carbonate.

The capture of atmospheric carbon dioxide is currently a large field of research.³⁶ Research by Jagadeesan et al, has shown that inorganic carbonates may be converted into useable methane gas.³⁷ As atmospheric carbon dioxide is likely being dissolved into solution then reacted into inorganic carbonates by the zinc porphyrin species presented in this paper, further research into the carbon capturing potential of these polymeric systems may have merit.

3. Conclusions

In summary, the series of porphyrin cored polymers and nanoparticles synthesized to study the secondary coordination sphere interactions of the metallo-organic core and polymeric scaffold formed adducts with sodium cyanide which had varying rates of reaction with DMF. Studying the reaction of cyanide and DMF in the presence of PCSP and PCPN species elucidated the significant role the functionalization and topology of the polymer scaffold played in the reactivity of the zinc porphyrin cyanide adduct. While all species catalyzed the reaction of sodium cyanide and DMF, the ester backboned PCSP and PCPN species formed the least reactive adducts of the series. The amide and ethanolamide species containing a greater number of potential hydrogen bond donors slightly increased the reactivity. The greatest difference in reactivity occurred in species with greater steric bulk. In addition, for all polymer species tested the folded particle topology formed more reactive cyanide adducts than the random coil topologies.

ASSOCIATED CONTENT

Supporting Information

Materials and instrumentation, full experimental procedures, NMR spectra, UV-Vis absorbance spectra, IR spectra and supporting figures.

AUTHOR INFORMATION

Corresponding Authors

*E-mail: erik.berda@unh.edu

*E-mail: sam.pazicni@chem.wisc.edu

Conflicts of interest

The authors declare no competing financial interest.

ACKNOWLEDGEMENTS

The authors thank the University of New Hampshire for financial support. In particular, E.B.B. thanks the Gloria G. and Robert E. Lyle Professorship. We also acknowledge the Army Research Office for support through award W911NF-14-0177 and W911NF-18-1-0216, NIST for support through award 70NANB15H060, and NSF for support via the NH EPSCOR NH BioMade Project Research Infrastructure Improvement Award #1757371.

References

(1) Poulos, T. L. Heme Enzyme Structure and

- Function. *Chem. Rev.* **2014**, *114* (7), 3919–3962. https://doi.org/10.1021/cr400415k.
- (2) Smith, A. T.; Pazicni, S.; Marvin, K. A.; Stevens, D. J.; Paulsen, K. M.; Burstyn, J. N. Functional Divergence of Heme-Thiolate Proteins: A Classification Based on Spectroscopic Attributes. *Chem. Rev.* 2015, 115 (7), 2532–2558. https://doi.org/10.1021/cr500056m.
- (3) Lin, Y. W. Structure and Function of Heme Proteins Regulated by Diverse Post-Translational Modifications. *Arch. Biochem. Biophys.* **2018**, *641* (November 2017), 1–30. https://doi.org/10.1016/j.abb.2018.01.0 09.
- (4) Zhao, M.; Wang, H. B.; Ji, L. N.; Mao, Z. W. Insights into Metalloenzyme Microenvironments: Biomimetic Metal Complexes with a Functional Second Coordination Sphere. *Chem. Soc. Rev.* 2013, 42 (21), 8360–8375. https://doi.org/10.1039/c3cs60162e.
- (5) Collman, J. P.; Fu, L. Synthetic Models for Hemoglobin and Myoglobin. Acc. Chem. Res. 1999, 32 (6), 455–463. https://doi.org/10.1021/ar9603064.
- (6) Phillips, S. E. V.; Schoenborn, B. P.
 Neutron Diffraction Reveals OxygenHistidine Hydrogen Bond in
 Oxymyoglobin. *Nature* **1981**, No. 5818, 81–82.
 https://doi.org/10.1038/292081a0.
- (7) Springer, B. A.; Egeberg, K. D.; Sligar, S. G.; Rohlfs, R. J.; Mathews, A. J.; Olson, J. S. Discrimination between Oxygen and Carbon Monoxide and Inhibition of Autooxidation by Myoglobin. Site-Directed Mutagenesis of the Distal Histidine. *J. Biol. Chem.* 1989, 264 (6), 3057–3060.
- (8) Pauling, L. Nature of the Iron-Oxygen Bond in Oxyhemoglobin. *Nature* **1964**,

- 203 (4941), 182-183.
- (9) Corwin, A. H.; Reyes, Z. Preparation and Properties of Imidazole Ferro- and Ferriprotoporphyrin Complexes 1. *J. Am. Chem. Soc.* **1956**, *78* (11), 2437–2439. https://doi.org/10.1021/ja01592a025.
- (10) Wang, J. H. HEMOGLOBIN STUDIES. II. A SYNTHETIC MATERIAL WITH HEMOGLOBIN-LIKE PROPERTY 1. J. Am. Chem. Soc. 1958, 80 (12), 3168–3169. https://doi.org/10.1021/ja01545a072.
- (11) Alben, J. O.; Fuchsman, W. H.;
 Beaudreau, C. A.; Caughey, W. S.
 Substituted Deuteroporphyrins. III.
 Iron(II) Derivatives. Reactions with
 Oxygen and Preparations from Chloroand Methoxohemins. *Biochemistry* **1968**,
 7 (2), 624–635.
 https://doi.org/10.1021/bi00842a018.
- (12) Chang, C. K.; Traylor, T. G. Solution
 Behavior of a Synthetic Myoglobin Active
 Site. J. Am. Chem. Soc. 1973, 95 (17),
 5810–5811.
 https://doi.org/10.1021/ja00798a088.
- (13) Anderson, D. L.; Weschler, C. J.; Basolo, F. Reversible Reaction of Simple Ferrous Porphyrins with Molecular Oxygen at Low Temperatures. J. Am. Chem. Soc. 1974, 96 (17), 5599–5600. https://doi.org/10.1021/ja00824a062.
- (14) Almog, J.; Baldwin, J. E.; Dyer, R. L.; Huff, J.; Wilkerson, C. J. Reversible Binding of Dioxygen to Mesoporphyrin IX Derivatives at Low Temperatures. *J. Am. Chem. Soc.* 1974, 96 (17), 5600–5601. https://doi.org/10.1021/ja00824a063.
- (15) Coliman, J. P.; Gagne, R. R.; Reed, C. A.; Halbert, T. R.; Robinson, W. T.; Lang, G. "Picket Fence Porphyrins". Synthetic Models for Oxygen Binding Hemoproteins. *J. Am. Chem. Soc.* **1975**, *97* (6), 1427–1439. https://doi.org/10.1021/ja00839a026.

- (16) Collman, J. P.; Zhang, X.; Wong, K.; Brauman, J. I. Dioxygen Binding in Iron and Cobalt Picnic Basket Porphyrins. J. Am. Chem. Soc. 1994, 116 (14), 6245– 6251. https://doi.org/10.1021/ja00093a026.
- (17) Lombardi, A.; Nastri, F.; Pavone, V. Peptide-Based Heme-Protein Models. Chem. Rev. 2001, 101 (10), 3165–3189. https://doi.org/10.1021/cr000055j.
- (18) Zhao, Z.; Wang, D.; Wang, M.; Sun, X.; Wang, L.; Huang, X.; Ma, L.; Li, Z. Proximal Environment Controlling the Reactivity between Inorganic Sulfide and Heme-Peptide Model. *RSC Adv.* **2016**, *6* (82), 78858–78864. https://doi.org/10.1039/c6ra14100e.
- (19) Tian, J.; Zhang, W. Synthesis, Self-Assembly and Applications of Functional Polymers Based on Porphyrins. *Prog. Polym. Sci.* **2019**, *95*, 65–117. https://doi.org/10.1016/j.progpolymsci. 2019.05.002.
- (20) Guo, J.; Liu, Y.; Zha, J.; Han, H.; Chen, Y.; Jia, Z. Enhancing the Peroxidase-Mimicking Activity of Hemin by Covalent Immobilization in Polymer Nanogels. *Polym. Chem.* 2021, 12 (6), 858–866. https://doi.org/10.1039/D0PY01465F.
- (21) Ji, T.; Xia, L.; Zheng, W.; Yin, G.; Yue, T.; Li, X.; Zhang, W.; Zhao, X.; Yang, H. Porphyrin-Functionalized Coordination Star Polymers and Their Potential Applications in Photodynamic Therapy. *Polym. Chem.* **2019**, *10* (45), 6116–6121. https://doi.org/10.1039/C9PY01391A.
- (22) Rodriguez, K. J.; Hanlon, A. M.; Lyon, C. K.; Cole, J. P.; Tuten, B. T.; Tooley, C. A.; Berda, E. B.; Pazicni, S. Porphyrin-Cored Polymer Nanoparticles: Macromolecular Models for Heme Iron Coordination. *Inorg. Chem.* **2016**, *55* (19), 9493–9496. https://doi.org/10.1021/acs.inorgchem. 6b01113.

- (23) Rodriguez, K. J. Modeling Secondary
 Coordination Sphere Interactions in
 Heme Proteins: From Small Molecule
 Ligands to Macromolecular PorphyrinCored Polymer Nanoparticles, University
 of New Hampshire, 2017.
- (24) Chiefari, J.; Chong, Y. K. B.; Ercole, F.; Krstina, J.; Jeffery, J.; Le, T. P. T.; Mayadunne, R. T. A.; Meijs, G. F.; Moad, C. L.; Moad, G.; et al. Living Free-Radical Polymerization by Reversible Addition–Fragmentation Chain Transfer: The RAFT Process. *Macromolecules* 1998, 31 (16), 5559–5562. https://doi.org/10.1021/ma9804951.
- (25) Perrier, S.; Takolpuckdee, P.
 Macromolecular Design via Reversible
 Addition-Fragmentation Chain Transfer
 (RAFT)/Xanthates (MADIX)
 Polymerization. J. Polym. Sci. Part A
 Polym. Chem. 2005, 43 (22), 5347–5393.
 https://doi.org/10.1002/pola.20986.
- (26) Frank, P. G.; Tuten, B. T.; Prasher, A.; Chao, D.; Berda, E. B. Intra-Chain Photodimerization of Pendant Anthracene Units as an Efficient Route to Single-Chain Nanoparticle Fabrication. *Macromol. Rapid Commun.* **2014**, *35* (2), 249–253. https://doi.org/10.1002/marc.201300677.
- (27) Liu, Y.; Pauloehrl, T.; Presolski, S. I.;
 Albertazzi, L.; Palmans, A. R. A.; Meijer,
 E. W. Modular Synthetic Platform for the
 Construction of Functional Single-Chain
 Polymeric Nanoparticles: From Aqueous
 Catalysis to Photosensitization. *J. Am.*Chem. Soc. 2015, 137 (40), 13096–
 13105.
 https://doi.org/10.1021/jacs.5b08299.
- (28) Zaia, J.; Annan, R. S.; Biemann, K. The Correct Molecular Weight of Myoglobin, a Common Calibrant for Mass Spectrometry. *Rapid Commun. Mass Spectrom.* **1992**, *6* (1), 32–36.

- https://doi.org/10.1002/rcm.129006010 8.
- (29) Kim, Y.-H.; Hong, J.-I. Ion Pair Recognition by Zn-Porphyrin/Crown Ether Conjugates: Visible Sensing of Sodium Cyanide. *Chem. Commun.* (Camb). **2002**, No. 5, 512–513. https://doi.org/10.1039/B109596J.
- (30) Yoon, H.; Lee, C. H.; Jeong, Y. H.; Gee, H. C.; Jang, W. D. A Zinc Porphyrin-Based Molecular Probe for the Determination of Contamination in Commercial Acetonitrile. *Chem. Commun.* 2012, 48 (42), 5109–5111. https://doi.org/10.1039/c2cc31149f.
- (31) Groves, P. Diffusion Ordered Spectroscopy (DOSY) as Applied to Polymers. *Polym. Chem.* **2017**, *8* (44), 6700–6708. https://doi.org/10.1039/c7py01577a.
- (32) Einstein, A. Motion of Suspended Particles in Stationary Liquids Required from the Molecular Kinetic Theory of Heat. *Ann. Phys.* **1905**, No. 17, 549–560. https://doi.org/10.1002/pmic.2009.0045 0.
- (33) N,N-Dimethylformamide | HCON(CH3)2 PubChem https://pubchem.ncbi.nlm.nih.gov/comp ound/dimethylformamide (accessed Feb 18, 2020).
- (34) Paul, R. C.; Sreenathan, B. R.
 Dimethylformamide as a Polar Solvent:
 Part IV Solubility, Solvate Formation &
 Solvolytic Reactions Of Substances in
 Dimethylformamide. *Indian J. Chem.*1966, 4 (9), 382–386.
- (35) Pohorecki, R.; Moniuk, W. Kinetics of Reaction between Carbon Dioxide and Hydroxyl Ions in Aqueous Electrolyte Solutions. *Chem. Eng. Sci.* **1988**, *43* (7), 1677–1684. https://doi.org/10.1016/0009-2509(88)85159-5.

- (36) Bui, M.; Adjiman, C. S.; Bardow, A.; Anthony, E. J.; Boston, A.; Brown, S.; Fennell, P. S.; Fuss, S.; Galindo, A.; Hackett, L. A.; et al. Carbon Capture and Storage (CCS): The Way Forward. *Energy Environ. Sci.* **2018**, *11* (5), 1062–1176. https://doi.org/10.1039/C7EE02342A.
- (37) Jagadeesan, D.; Eswaramoorthy, M.; Rao, C. N. R. Investigations of the Conversion of Inorganic Carbonates to Methane. **2009**, 878–882. https://doi.org/10.1002/cssc.200900152

12